



Heterogeneous & Homogeneous & Bio- & Nano-

CHEM **CAT** CHEM

CATALYSIS

Accepted Article

Title: Facile in situ encapsulation of highly dispersed Ni@MCM-41 for the trans-decalin production from hydrogenation of naphthalene at low temperature

Authors: Xiaoyun Song, Qingxin Guan, Yu Shu, Xiaojing Zhang, and Wei Li

This manuscript has been accepted after peer review and appears as an Accepted Article online prior to editing, proofing, and formal publication of the final Version of Record (VoR). This work is currently citable by using the Digital Object Identifier (DOI) given below. The VoR will be published online in Early View as soon as possible and may be different to this Accepted Article as a result of editing. Readers should obtain the VoR from the journal website shown below when it is published to ensure accuracy of information. The authors are responsible for the content of this Accepted Article.

To be cited as: *ChemCatChem* 10.1002/cctc.201801788

Link to VoR: <http://dx.doi.org/10.1002/cctc.201801788>

WILEY-VCH

www.chemcatchem.org



FULL PAPER

Facile in situ encapsulation of highly dispersed Ni@MCM-41 for the trans-decalin production from hydrogenation of naphthalene at low temperature

Xiaoyun Song,^[a] Qingxin Guan,^{*[a]} Yu Shu,^[a] Xiaojing Zhang,^[a] and Wei Li,^{**[a] [b]}

Abstract: Ni@MCM-41 catalyst that has uniformly distributed, highly dispersed Ni nanoparticles (about 2.3 nm) was designed and successfully synthesized by in situ encapsulation of Ni in the channels of MCM-41. This catalyst exhibits excellent thermal stability and hydrogenation activity. Water insoluble nickel acetylacetonate (Ni(acac)₂) was first dissolved aqueous solution of cetyltrimethyl ammonium bromide (CTAB) and encapsulated in micelles of CTAB. Sodium silicate was used as a silicon source to rapidly hydrolyze and then wrap on the micelle surface to synthesize the MCM-41 zeolite. The MCM-41 zeolite encapsulating Ni(acac)₂ was synthesized within a short time (4 h) at 120 °C. Compared with conventional supported catalysts, thus 3 wt.% Ni@MCM-41 has ultra-small uniformly distributed Ni nanoparticles and exhibits improved activity for the hydrogenation of naphthalene to decalin at very low reaction temperatures. The TOF and the apparent activation energy of Ni@MCM-41 and the conventional catalysts (Ni/MCM-41 and Pt/MCM-41) were evaluated and compared. And the catalysis mechanism was analyzed. Furthermore, this Ni@MCM-41 catalyst offers an additional advantage of selectivity in decalin isomerization; 92% trans-decalin selectivity was achieved at a wide temperature range.

Introduction

Aromatic compounds present in diesel lead to diesel with a lower cetane number and increased particulate pollutants in exhaust gases; hence, the removal of aromatic hydrocarbons from fuel is considered an urgent task. Naphthalene is generally used as a model compound for the hydrodearomatization (HDA) reaction. Naphthalene is also a major component of light cycle oil and coal tar, and it can be hydrogenated to produce tetralin and decalin. Hence, for the reasons of producing environmental friendly fuels and meeting demands for the conversion of fine chemicals from

coal-based raw materials, much effort has gone into the development of highly efficient supported catalysts for HDA. According to many published papers, supported noble metal catalysts (e.g., Ru,^[1] Pd,^[2] and Pt^[3]) exhibit excellent hydrogenation performance; however, unfortunately, large-scale industrial applications are severely limited because of the high cost and low reserves of noble metals. Furthermore, noble metal catalysts are easily poisoned by sulfur compounds present in fossil feedstock. In the research for less costly supported catalysts, Ni catalysts have attracted much attention because of their low-cost, rich-reserves, and sulfur-tolerance.^[4] Ni catalysts have been widely reported; they have significant potential applications in heterogeneous catalysis.^[5] Many unsupported Ni-based particles with high dispersion and uniform size distribution have been synthesized, and they often exhibit catalytic performances.^[6] However, these Ni materials tend to be unstable toward sintering or aggregation in catalytic reactions; hence, they are unsuitable for heterogeneous catalysis, especially for catalytic reactions in a fixed-bed reactor. The idea of the preparation of supported Ni catalysts is one of the themes of heterogeneous catalytic HDA research. Of note here is that the hydrogenation of aromatic compounds is an exothermic reaction and low reaction temperature is more beneficial to the conversion of aromatics. Unfortunately, a supported Ni catalyst has low activity at low temperature and it is unstable during the hydrogenation process.^[7] Therefore, how to improve the low temperature activity and stability of a supported Ni catalyst remains a significant challenge.

For a supported catalyst, the particle size of the active component/s is a crucial parameter, as it influences the activity, selectivity, and lifetime of the catalyst.^[8] Smaller metal nanoparticles are often more effective because they are able to expose more active sites. Although many methods have been described for the synthesis of supported catalysts with small metal particles, results indicate that their use still leads to uncontrollable size distribution or relatively poor stability in catalytic processes.^[9] To overcome existing limitations, encapsulation is considered an attractive strategy to design highly dispersed metal nanoparticle catalysts with excellent stability.^[10] Jian Zhang et al.^[11] constructed a defined structure (Pd@Beta) by fixing Pd nanoparticles inside Beta zeolite, which exhibited enhanced hydrogenation selectivity and stability. This work offered a new concept for the design of durable catalysts with high selectivity. Mesoporous silica type MCM-41, possesses a large surface area, narrow pore size distribution, and good thermal stability. MCM-41 is therefore considered as an ideal catalyst support candidate. The synthetic approach to MCM-41 involves multidentate binding

[a] Dr. X. Song, Prof. Q. Guan, Y. Shu, X. Zhang, Prof. W. Li
College of Chemistry, State Key Laboratory of Elemento-Organic
Chemistry, Key Laboratory of Advanced Energy Materials Chemistry
(Ministry of Education), Nankai University, Tianjin 300071, China
E-mail: qingxinguan@nankai.edu.cn; weili@nankai.edu.cn

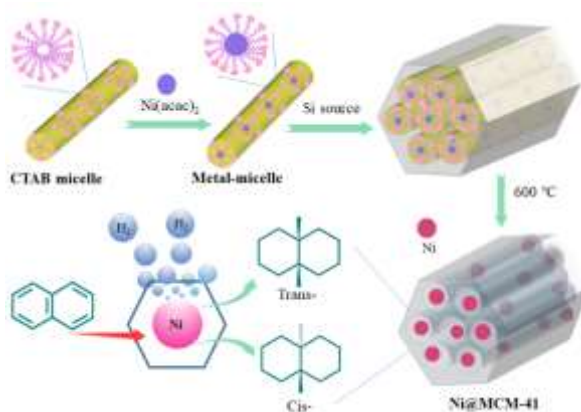
[b] Prof. W. Li
Collaborative Innovation Center of Chemical Science and
Engineering (Tianjin), Nankai University, Tianjin 300071, China

Supporting information for this article is given via a link at the end of the document.

FULL PAPER

of silicate oligomers to the cationic surfactant and charge density matching of surfactant–silicate.^[12] Therefore, MCM-41 can be considered a good candidate for supporting metal nanoparticles inside the pores. Indeed, it has often been used as a support for generating noble metal nanoparticles. Xijie Lin and coworkers^[13] introduced Pd nanoparticles into the channels of MCM-41, which led to the formation of highly dispersed and stable Pd species. This synthetic method may be useful for non-noble metals with nanosizes <5 nm, which are otherwise difficult to reach and control.

Here, we demonstrate a simple and efficient method for the in situ encapsulation of Ni nanoparticles in MCM-41 channels. The detailed synthesis route is shown in Scheme 1. In this strategy, the cetyltrimethyl ammonium bromide (CTAB) surfactant is not only used as a micelle template for the formation of MCM-41, but also utilized for grafting Ni species effectively. Sodium silicate is used as a silicon source to rapidly hydrolyze and then encapsulate the micelle to synthesize the MCM-41. Ultimately, the newly prepared Ni@MCM-41 catalyst has ultra-small uniformly distributed Ni nanoparticles, and completely different activity and selectivity compared with the corresponding conventional Ni/MCM-41.



Scheme 1. Illustration of the in situ Ni@MCM-41 synthesis and HDA reaction.

Results and Discussion

ICP results (Table S1) reveal that the actual Ni loadings in the Ni@MCM-3.0 and Ni@MCM-1.5 samples are 3.0% and 1.5%, respectively. In terms of appearance, the Ni@MCM-*x* is a different colour to Ni/MCM-41, synthesized using a traditional impregnation method. The color of the matrix material (MCM-41) is white, whereas the color of Ni/MCM-41 is dark black. The latter may be attributed to the Ni species located on the surface of the sample.^[12] However, Ni@MCM-*x* shows a light gray color. This is attributed to not much Ni present on the outer surface. This result is taken as an initial indication of the encapsulation of Ni in the channels of MCM-41. A similar appearance of Pd nanoparticles supported on B-MCM-41 has been reported by Chatterjee.^[12] Successful synthesis of the mesoporous MCM-41 structure was confirmed by XRD patterns (Figure 1). Three characteristic peaks

of the hexagonal structure for Ni@MCM-*x* are well discerned in small-angle XRD patterns. Thus, the incorporation of Ni by the in situ encapsulation method does not destroy the symmetry of the porous framework. The intensities of the major peaks decrease slightly, however, with increasing Ni content, which is probably because a small fraction of the mesopores are filled, and block Ni incorporation. Besides this, there is a slight change in the diffraction peak positions for Ni@MCM-*x* compared with blank MCM-41, which is probably related to a slightly larger pore size for the Ni@MCM-*x*.

Furthermore, wide-angle XRD patterns of Ni@MCM-*x* were also detected and compared with Ni/MCM-41 (see Figure 1, inset). Typical peaks of Ni appear in the XRD patterns of Ni/MCM-41. However, the patterns of Ni@MCM-*x* samples only reveal a broad SiO₂ diffraction peak; no clear peak belonging to Ni is observed. This result indicates that the Ni particles of Ni@MCM-*x* may be too small and highly dispersed in the channels to be detected. And this supposition is confirmed by the dispersion results calculated from CO chemisorption. As Table 1 shows, the dispersion of Ni@MCM-*x* is much higher than that of Ni/MCM-41, which suggests that our encapsulation method can effectively improve the dispersion of Ni particles.

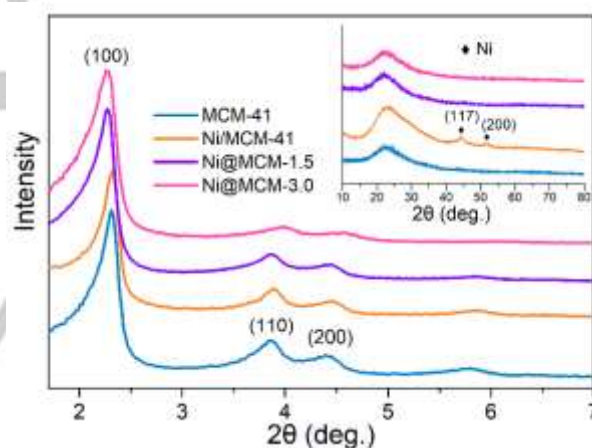


Figure 1. Small-angle XRD patterns of MCM-41, Ni/MCM-41, and Ni@MCM-*x* (*x*=1.5, 3.0). Inset: wide-angle XRD patterns.

As Figure 2 shows, the N₂ absorption–desorption isotherms of samples are typical IV type with monolayer adsorption, which is a typical characteristic of mesoporous materials. There is a sharp increase in N₂ adsorption within a narrow range of relative pressure (0.3 – 0.4), arising from capillary condensation of N₂ inside the mesopores. It is well known that a steep hysteresis loops between adsorption and desorption always indicates a narrow mesopore size distribution. For all samples, the adsorption path coincides with the corresponding desorption path and no hysteresis loops are observed. This is in accordance with what reported for MCM-41 in the literature.^[14] This result suggests that all samples here possess ordered mesopores. This is consistent with the pore diameter distribution shown in Figure 2 (inset). Textural properties of samples are tabulated in Table 1. There is

FULL PAPER

only a slight decrease in the surface area (S_{BET}) of Ni@MCM-1.5 ($902 \text{ m}^2 \text{ g}^{-1}$) compared with blank MCM-41 ($969 \text{ m}^2 \text{ g}^{-1}$), owing to Ni incorporation. Although the S_{BET} of Ni@MCM-3.0 shows an decrease of 14% with respect to MCM-41, its S_{BET} is still much higher than that of Ni/MCM-41 (24%). Interestingly, the average pore size decreases slightly from 2.9 to 3.1 nm, which may be attributed to the encapsulation of Ni. This result is in good agreement with that the XRD peaks shift to a smaller angle and the pore diameter distribution (Figure 2 inset) shift to a larger size. Therefore, the introduction of Ni particles affects the MCM-41 structure to some extent. Notwithstanding such a small difference, the overall results of N_2 sorption suggest that Ni@MCM-x possess a mesoporous structure with ordered channels.

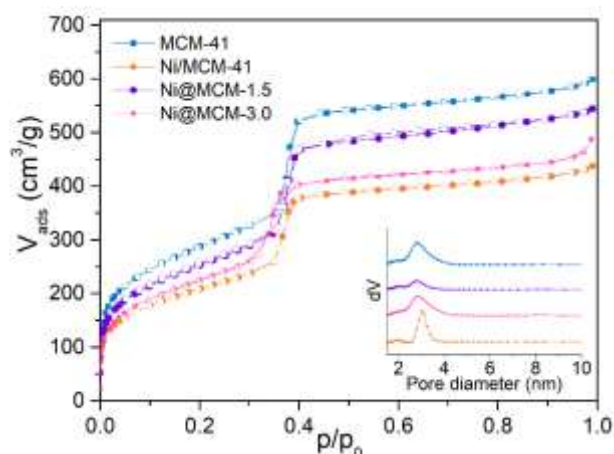


Figure 2. Nitrogen adsorption-desorption isotherms and pore diameter distribution (inset) of as-prepared samples.

Table 1. Textural properties of samples.

Sample	$S_{\text{BET}}^{[a]}$ (m^2/g)	$d^{[b]}$ (nm)	$V_{\text{total}}^{[c]}$ (cm^3/g)	Metal dispersion ^[d]
MCM-41	969	2.4	0.93	--
Ni/MCM-41	738	2.4	0.68	36%
Ni@MCM-1.5	902	2.4	0.84	51%
Ni@MCM-3.0	823	2.6	0.75	50%

[a] surface area was calculated with BET method. [b] average pore size determined by means of BJH method. [c] total pore volume obtained at $P/P_0 = 0.999$. [d] was estimated according to the number of CO molecules adsorbed and the CO uptake was listed in Table 2.

TEM images are shown in Figure 3. They not only confirm the above results, but also give direct insight into the presence and size distribution of Ni nanoparticles, including the structural properties of samples. The ordered mesoporous structure of 'blank' MCM-41 (Figure 3a) can be clearly distinguished. In an image of Ni/MCM-41 (Figure 3b), many bulky Ni particles exist on

the external surface of MCM-41. By contrast, in Ni@MCM-x (Figure 3c, e), the Ni nanoparticles are small (average size 2.3 nm); almost no large particles were found. Most Ni nanoparticles are confined within the channels of MCM-41, which indicates that the channels of MCM-41 play a role in the encapsulation of Ni nanoparticles. More importantly, Ni nanoparticles remain highly dispersed in the channels of MCM-41, although the Ni content increases from 1.5 wt.% to 3.0 wt.%. Results also indicate that the Ni nanoparticles of Ni@MCM-3.0 and Ni@MCM-1.5 are the same size. This size is controllable and does not unaffected by the Ni loadings. The Ni dispersion was further confirmed by STEM pictures, including BF and HAADF images (Figure 4). Furthermore, the existence of Ni in Ni@MCM-x was identified by EDS (Figure 3d). Hence, we can confidently state that, as expected, our synthesis route is effective in encapsulating Ni into the channels of MCM-41.

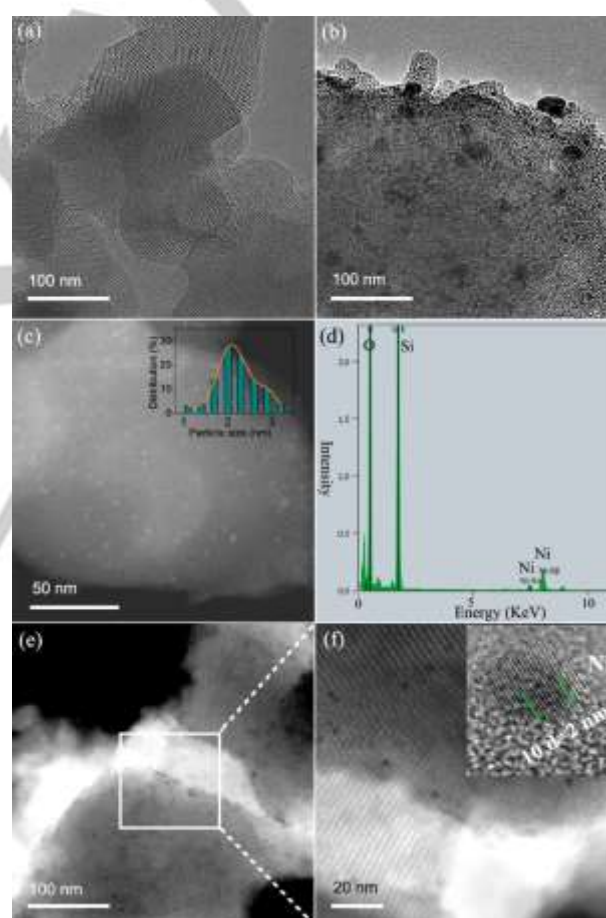


Figure 3. TEM images of (a) MCM-41, (b) Ni/MCM-41, STEM images of (c) Ni@MCM-3.0 under a bright field operation mode and its EDS analysis (d), and STEM images of (e, f) Ni@MCM-1.5 under dark field mode. Inset of (f): HRTEM of Ni nanoparticle gives the crystal plane of the (111) for Ni.

The mechanism can be rationalized by the role of CTAB surfactant in the grafting of Ni species inside the mesopores. The synthesis process and mechanism are shown in Scheme 1. In our

FULL PAPER

method, CTAB is used as micelle template for the formation of MCM-41, and $\text{Ni}(\text{acac})_2$ is employed as the source of Ni species. Interestingly, a clear solution is obtained when water insoluble $\text{Ni}(\text{acac})_2$ is dissolved in aqueous solution of CTAB as a result of the interaction between $\text{Ni}(\text{acac})_2$ and CTAB. As is well known, a micelle of CTAB can form in aqueous solution as a result of the ordered uniform aggregation of its organic group. Acetylacetonate (acac) ligand of $\text{Ni}(\text{acac})_2$ can interact with the organic group of CTAB,^[15] and hence, the $\text{Ni}(\text{acac})_2$ can enter the hydrophobic core of surfactant micelles. In other words, Ni species are encompassed by CTAB and grafted into micelles.

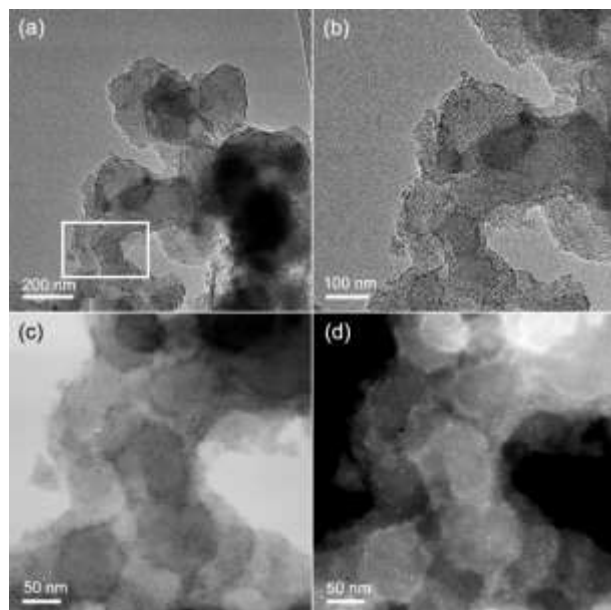


Figure 4. TEM (a, b) and STEM images under bright (c) and dark (d) mode for Ni@MCM-3.0.

To gain a better understanding of the existent state of Ni species in the formation process of MCM-41, a parallel experiment was carried out. In this experiment, to avoid interference from a silica precipitate and simulate the alkaline conditions, NaOH was used as a replacement for sodium silicate. The pH value of the $\text{Ni}(\text{acac})_2/\text{CTAB}$ solution was adjusted from 8 to 13 by adding NaOH. The UV-vis spectra of the solution before (pH = 8) and after (pH = 13) adding NaOH, as well as an aqueous solution of CTAB, are compared in Figure 5. There is no apparent change, irrespective of whether the pH value was 8 or 13, which illustrates that alkaline conditions have little effect on $\text{Ni}(\text{acac})_2$. In other words, the Ni species remains stable within CTAB micelles of a MCM-41 precursor. In the next step, when the precursor was calcined at 600 °C in air and reduced in H_2 , the organic components were decomposed. Meanwhile, Ni atoms were released and aggregated together. Therefore, Ni particles were generated and confined within the channels of MCM-41, as observed in the TEM images.

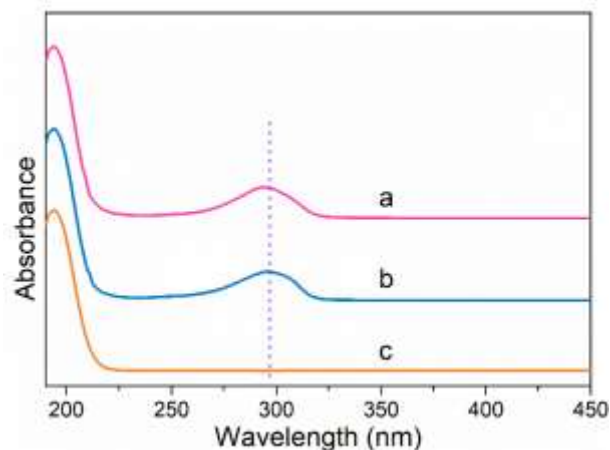


Figure 5. The UV-vis spectra of different solutions: solution of $\text{Ni}(\text{acac})_2$ and CTAB before (a) and after (b) adding NaOH, and CTAB aqueous (c).

The XRD (Figure S1) and XPS (Figure S2) results of Ni/MCM-41 and Ni@MCM-3.0 before reduction show that Ni species are in the form of Ni oxide in both samples before reduction. The XPS spectra of Ni/MCM-41 and Ni@MCM-3.0 samples after reduction were recorded under identical conditions; the results are shown in Figure 6. The predominant peaks, centered at 852.7 eV, 870.8 eV, and 860.2 eV, can be assigned to metallic Ni (Ni^0) 2p_{3/2}, Ni^0 2p_{1/2}, and a satellite peak. A further peak at 854.6 eV is assigned to Ni^{2+} , which may be attributed to the surface NiO.^[16] XPS is commonly used to analyze the distribution of elements within a surface of (to the depth of) several nanometers. When considering a reason why the Ni intensity of the XPS spectra of Ni@MCM-3.0 is too weak to distinguish, it is possible that most of the Ni nanoparticles are confined and highly dispersed in the channels of MCM-41, which means that the Ni nanoparticles in this sample is lower than the detection limit of XPS. The metal Ni in Ni@MCM-41 after reduction has been confirmed by HRTEM results (Figure 3f). In a word, the XPS results combined with characterization of wide-angle XRD, and HRTEM, confirm the metal Ni in Ni/MCM-41 and Ni@MCM-3.0 samples after reduction. Therefore, being reduced in H_2 at 600 °C for 2 hours can ensure a complete reduction of nickel oxides.

FULL PAPER

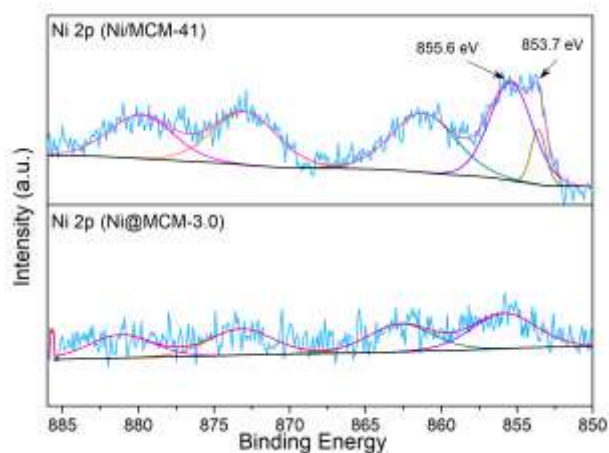


Figure 6. XPS spectra of Ni/MCM-41 and Ni@MCM-3.0 samples.

The advantage of our encapsulation method is that not only are highly dispersed Ni nanoparticles generated inside the channels of MCM-41, but also the sintering of Ni nanoparticles is prevented. Therefore, the thermal stability of this catalyst is obviously improved. Generally, high temperature treatment leads to an aggregation or growth of Ni nanoparticles. After treatment at 800 °C for 1 h, the conventional Ni/MCM-41 is found to have Ni nanoparticles with larger particle sizes (Figure 7a) than in the as-prepared sample (Figure 3b). This may be caused by the weak interaction between Ni²⁺ and MCM-41, which causes the Ni nanoparticles to be sintered and aggregated on the external surface of MCM-41 during the calcination and reduction process. On the other hand, Ni nanoparticles in Ni@MCM-3.0 (Figure 7b) remain inside channels, with no sintering after thermal treatment, and the particle size is similar to that of the fresh sample (Figure 3c). Therefore, as expected, Ni@MCM-3.0 shows extraordinary thermal stability. This result is attributed not only to the fact that most of the Ni particles are confined within the channels, but also to the strong interaction between Ni and MCM-41 support.

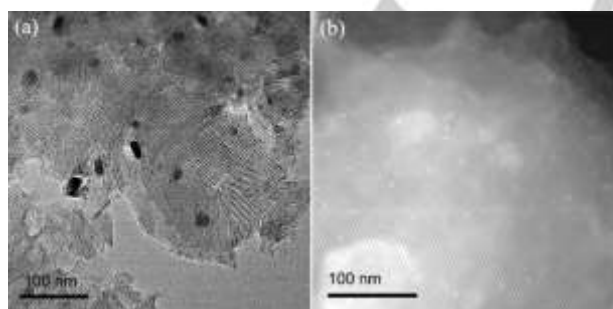


Figure 7. TEM images of (a) Ni/MCM-41 and (b) Ni@MCM-41-3.0 after thermal treatment.

H₂-TPR is an effective technique for obtaining information on the interaction strength between metal species and supports, in addition to the reducibility of different metal species. Therefore,

the interaction strength between Ni and a MCM-41 support can be determined according to the reduction temperature. All H₂-TPR profiles of samples (Figure 8) show two reduction stages. Obviously, Ni@MCM-3.0 and Ni@MCM-1.5 samples show similar peak profiles, suggesting the same interaction between Ni and MCM-41 in both samples. Compared with Ni/MCM-41, both stages of Ni@MCM-x are shifted to a higher temperature, which indicates a stronger interaction between Ni and MCM-41 in both samples. This strong interaction leads to a fixation of Ni into MCM-41 channels in the Ni@MCM-41 composite. The extraordinary thermal stability of Ni@MCM-3 (Figure 7) can be reasonably attributed to the fixed structure of Ni and the silica support.^[17] According to a previous study, a low reduction temperature peak is associated with bulky and aggregative NiO particles on the surface of MCM-41.^[18] And a peak at higher temperature is attributed to smaller and more dispersed NiO particles, which interact strongly with the mesoporous MCM-41 support. Hence, from this result, combined with the above analysis of thermal stability (Figure 7), we can summarize by stating that the function of confining Ni within the channels of MCM-41 results in not only high dispersion of Ni particles, but also the prevention of these particles from aggregation and sintering.

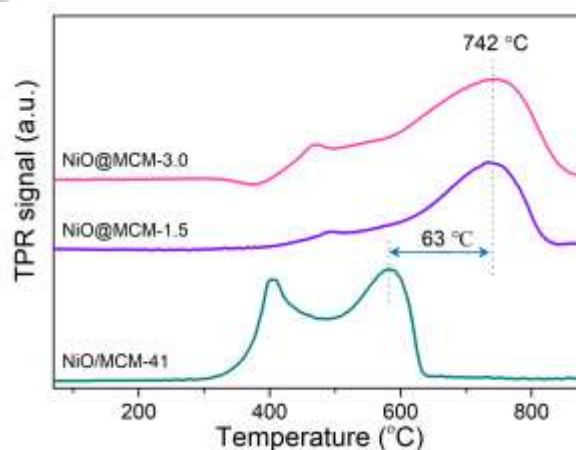


Figure 8. H₂-TPR of Ni/MCM-41, and Ni@MCM-x samples.

It is well known that the dissociative hydrogen adsorption capacity of a catalyst is related to its electronic structure.^[19] This, combined with the H₂-TPR results, we can deduce that the electronic properties of Ni can be modified through this in situ method.

Test (Table S2) shows that nickel oxide possesses almost no activity on hydrodearomatization. Based on the results of H₂-TPR, all catalysts described here in this manuscript were reduced by H₂ after 2 h at 600 °C; the complete reduction of NiO before the HDA reaction is therefore ensured. It is acknowledged that the size of the metal component is vital to the catalytic efficiency, and that the thermal stability is important for heterogeneous catalysis; therefore, an enhanced hydrogenation performance can be expected here.

FULL PAPER

Naphthalene was used as a model compound for the HDA reaction. The catalytic performance of Ni@MCM-x was evaluated by the hydrogenation of naphthalene. The hydrogenation process is illustrated in Figure 9,^[9a] and the structure models optimized by DFT method are shown in Figure S3. The main product is fully saturated decalin and the by-product is partially hydrogenated tetralin. For comparison, conventional catalysts were also tested, specifically, 3 wt.% Ni/MCM-41 and 0.3 wt.% Pt/MCM-41 (TEM, Figure S4). HDA results indicate that the conversion and selectivity of all catalysts tend to increase at temperatures below 260 °C, but decrease above that. This is because the hydrogenation of aromatics is an exothermic reaction, and a low temperature is thermodynamically favored. At lower temperatures (140 – 260 °C), Ni@MCM-3.0 displays 100% conversion as well as 100% selectivity for decalin (Figure 10). However, the highest selectivity for decalin, by Ni/MCM-41, is only 92.3%. Ni/MCM-41 shows incomplete conversion of naphthalene below 220 °C. Therefore, in terms of HDA activity, it is considerably improved by encapsulating Ni into the channels of MCM-41. In terms of decalin selectivity, that exhibited by Ni@MCM-3.0 is much higher than that of the Pt/MCM-41 catalyst over the temperature range considered in the present study (Figure 10b). Overall, the conversion and decalin selectivity are 100% over quite a wide range of test temperatures (140 – 260 °C) for Ni@MCM-3.0. However, for Ni/MCM-41 and Pt/MCM-41, there is a sharp decline when the temperature decreases as a result of a decrease in catalytic activity at low temperatures. Ni@MCM-3.0 displays outstanding activity not only at higher, but also lower temperatures.

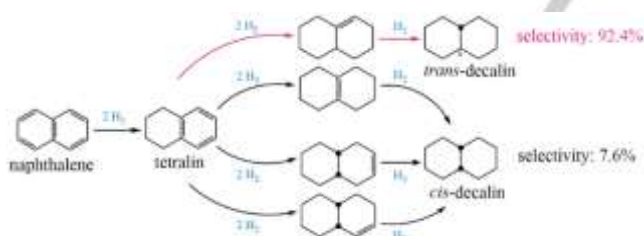


Figure 9. Reaction pathway of naphthalene hydrogenation.

To study the efficacy of the catalysts further, the TOFs were calculated and compared (Table 2). Pt/MCM-41 shows optimal catalytic efficiency with the highest TOF value (65.8 h⁻¹) because of the excellent catalysis nature of the noble metal. Ni@MCM-3.0 (28.0% conversion) exhibits a much higher conversion than 0.3 wt.% Pt/MCM-41 (10.3% conversion). This is a rather exciting result, given that the TOF of Pt/MCM-41 catalyst is twice that of Ni@MCM-41 catalyst. It is acknowledged that noble components are usually used with a loading of <1% in industrial applications because of their high cost and low reserves. This is in contrast to the loading of non-noble metals, which tends to be >10%. So the above results about 3 wt.% Ni@MCM-41 and 0.3 wt.% Pt/MCM-41 suggest that Ni@MCM-41 has great potential as an alternative to noble metals in heterogeneous catalysis.

Furthermore, the apparent activation energy (E_a) of catalyst was evaluated from the Arrhenius plots (Figure 11) at naphthalene conversion <20% to avoid the mass diffusion limitation. E_a values are tabulated in Table 3. As expected, Pt/MCM-41 exhibits the highest activity with the lowest E_a . Ni@MCM-3 displays a lower E_a compared with Ni/MCM-41, suggesting a higher catalytic performance. This indicates that the encapsulation of Ni in MCM-41 channels is greatly beneficial for the development of catalytic activity. These results further confirm the advantage of encapsulation of Ni. Of note is that these E_a results are in good agreement with the results of catalytic activity.

Table 2. TOF of HDA at 120 °C, LHSV = 3 h⁻¹.

Catalysts	Metal content	CO _{uptake} (μmol g ⁻¹)	Conversion	TOF (h ⁻¹)
Ni@MCM-3.0	3.0%	6.1	20.0%	31.4
Ni/MCM-41	3.0%	4.4	12.6%	18.3
Pt/MCM-41	0.3%	1.0	10.3%	65.8

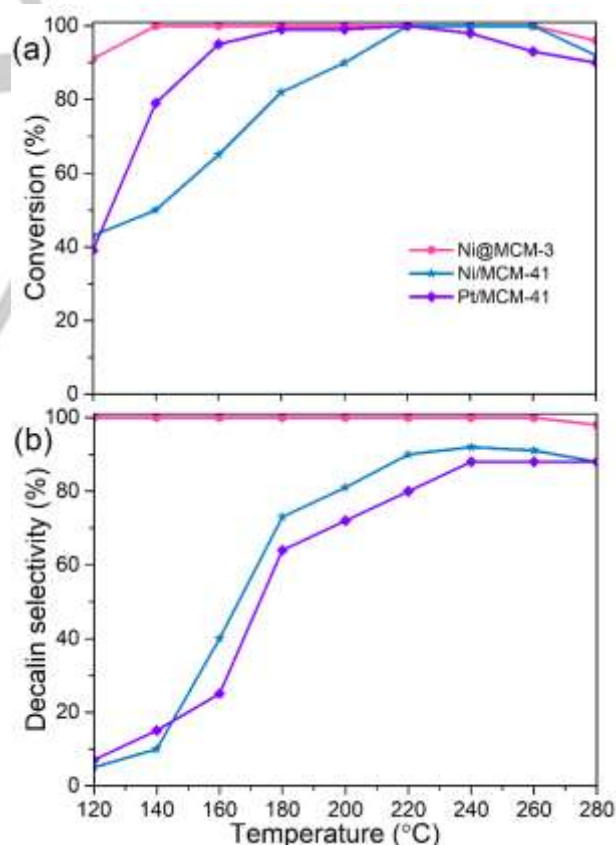


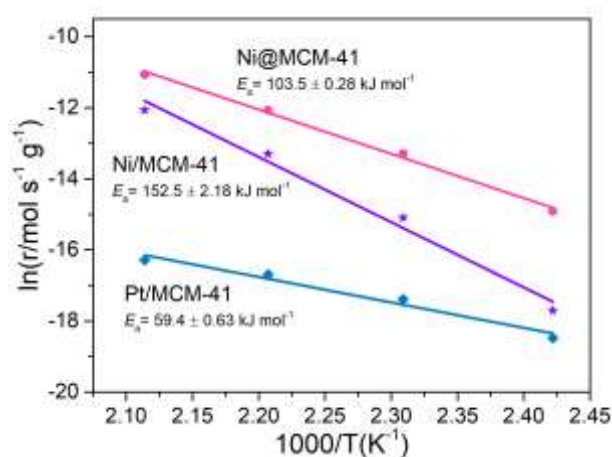
Figure 10. (a) Conversion and (b) selectivity of catalysts at LHSV = 1 h⁻¹.

FULL PAPER

Table 3. The trans-decalin selectivity of catalysts at the same conversion of 100%.

Catalysts	E _a (kJ mol ⁻¹)	Trans-selectivity ^a (%)					
		160 °C	180 °C	200 °C	220 °C	240 °C	260 °C
Ni@MCM-3.0	103.5	92.4	92.4	92.4	92.3	92.3	92.4
Ni/MCM-41	152.5	--	--	--	80.1	86.3	86.0
Pt/MCM-41	59.4	--	57.1	56.9	58.7	--	--

[a] The trans-decalin selectivity calculated by calculating the percentage of trans-decalin in decalin (trans- + cis-) product.

**Figure 11.** Arrhenius plots of catalysts at LHSV = 3 h⁻¹.

According to the analytical results described above, we can confidently state that the encapsulation structure of Ni@MCM-3.0 can significantly improve the catalysis efficiency of HDA. Ni particles in Ni@MCM-3.0 are ultra-small in size and highly dispersed but much larger and agglomerated in Ni/MCM-41, which has been confirmed in TEM analysis. In addition, Ni@MCM-3.0 shows a much higher CO_{uptake} (Table 2) than that of Ni/MCM-41, suggesting Ni@MCM-3.0 possesses more active sites than Ni/MCM-41. Considering that the Ni@MCM-3.0 and Ni/MCM-41 catalysts have similar Ni loadings and the same mesoporous silica support, the higher activity of Ni@MCM-3.0 can be reasonably attributed to its smaller encapsulated Ni particles, which expose more active sites.^[20] Besides, XPS results of samples before (Figure 6) and after (Figure S5) catalysis suggest that there is no Ni species change occurred in the hydrogenation. As illustrated in Figure 8, decalin has two isomers, trans-decalin and cis-decalin. Interestingly, when at a same conversion of 100%, Ni@MCM-3.0 shows a significantly higher catalytic selectivity for trans-decalin than other tested catalysts (Table 3). Ni@MCM-3.0 maintains a selectivity for trans-decalin of 92% over the reaction temperature range of 160 – 260 °C. On the contrary, both Ni/MCM-41 and Pt/MCM-41 catalysts have much lower trans-decalin selectivity. It can be concluded that the

encapsulation of Ni particles inside the channels of MCM-41 has a beneficial effect on trans-decalin selectivity.

To the best of our knowledge, there is, as yet, no confirmed mechanism for isomer selectivity.^[21] Some direct evidence can now be used to address this (the reaction pathway). We propose the following reason for isomer selectivity. It can be speculated that the in situ synthesis method causes a stronger electronic interaction between Ni and MCM-41, as determined from the H₂-TPR results (Figure 8), which subsequently causes an increased electron density of the Ni species.^[12] Hence, the Ni species can interact more strongly with HDA intermediates adsorbed on the MCM-41 support. These intermediates are formed after the hydrogenation of tetralin to decalin. This hydrogenation step is structure sensitive. More importantly, it is a key step in decalin isomer selectivity.^[22] Ni@MCM-3.0 shows remarkable trans-decalin selectivity, which might be the result of the stronger adsorption of the intermediate (A), as illustrated in Figure 9. Furthermore, the encapsulation structure of Ni@MCM-3.0 facilitates the adsorption and enrichment of naphthalene in the channels of MCM-41 and promotes the desorption of trans-decalin rather than the cis-decalin or tetralin by-product.^[17] Overall, confining Ni within the channels of MCM-41 not only results in excellent catalysis activity, but also offers an advantage in terms of isomerization selectivity.

As is well known, the HDA reaction is one of the most important reactions used in modern-day oil refineries; decalin is produced from naphthalene. Generally, decalin is manufactured commercially, using a conventional HDA catalyst, and the product is almost a 50/50 mixture of trans-/cis-decalin. Many published papers have focused on the isomerization activity of supported metal catalysts in naphthalene hydrogenation,^[23] and those results indicate that high isomerization selectivity is always associated with the use of noble metals and/or harsh reaction conditions. Unfortunately, a trans-decalin selectivity which >92% is rarely achieved in such processes. Therefore, indications are that the Ni@MCM-3.0 catalyst may be a promising and effective alternative to noble metal catalysts in selective naphthalene hydrogenation.

Conclusions

FULL PAPER

In summary, an efficient and simple in situ method for the controlled encapsulation of Ni particles inside the channels of MCM-41 is reported. In this method, Ni(acac)₂ is employed as Ni source and grafted into the micelle template of CTAB. Sodium silicate is used as a silicon source to rapidly hydrolyze and then wrap on the micelle surface to synthesize MCM-41 zeolite. The MCM-41 zeolite encapsulating Ni(acac)₂ is synthesized at 120 °C within 4 h, which also significantly reducing the synthesis time. Homogeneously distributed Ni nanoparticles with an average size of 2.3 nm are formed and highly dispersed inside the pores of MCM-41 after removal of the template. As a result of the encapsulation, Ni@MCM-41 displays extraordinary thermal stability. Results of evaluation of catalytic activity indicate that 3 wt.% Ni@MCM-41 is an excellent catalyst for the HDA reaction of naphthalene to decalin. Its activity is even much higher than that of conventional 0.3 wt.% Pt/MCM-41 catalysts. Furthermore, it shows high isomer selectivity for decalin; 92% trans-decalin selectivity was recorded over a wide reaction temperature range of 160 – 260 °C. Due to its superior catalytic performance together with its simple synthesis route, this Ni@MCM-41 catalyst can be potentially applied to a large-scale production. This in situ method should not only largely simplify synthesis routes to supported metal catalysts, but also lead to improved catalytic activity. Hence, it may open opportunities for the development of highly active non-noble metal catalysts for efficient heterogeneous catalysis and the selective production of isomers.

Experimental Section

Sodium silicate (Na 0.7 mol kg⁻¹, Si 2.5 mol kg⁻¹, H₂O 80 wt.%; >99%) was purchased from Tianjin Chemicals (Tianjin, China) Scientific Company. Nickel acetylacetonate (Ni(acac)₂), naphthalene, CTAB, nickel nitrate hexahydrate, and H₂PtCl₆ were purchased from Shanghai Sigma-Aldrich (Shanghai, China). All materials were used as received. Deionized water was used as throughout.

Catalyst preparation

Ni@MCM-41 was prepared by mixing sodium silicate, CTAB, deionized water and Ni(acac)₂ in a molar ratio of 1 SiO₂ : 0.12 CTAB : 40 H₂O : 0.003-0.004 Ni(acac)₂. The synthesis was carried out as follows. First, CTAB and an appropriate quantity of Ni(acac)₂ were dissolved in water under strong agitation until a clear solution was obtained. The resulting mixture was held at 75 °C for 0.5 h. Second, sodium silicate was added. After further agitation for 0.5 h, the resulting solution was cooled to 60 °C. Third, the pH value of the solution was adjusted to 10 by the dropwise addition of HCl. After further agitation for 3 h, the mixture was transferred to an autoclave and heated to 130 °C for 5 h. Fourth, the solid product was filtered, washed five times with deionized water, and then dried at 80 °C. Finally, the prepared material was calcined in air at 600 °C for 5 h to fully remove the CTAB template to yield NiO/MCM-41. The Ni@MCM-41 catalyst was obtained after reduction at 600 °C for 2 h in a H₂ flow. It was then passivated in a gas mixture (99.5% N₂ and 0.5% O₂) at 100 °C for 4 h before exposure to air. Ni@MCM-41 catalysts with 3.0 wt.% and 1.5 wt.% Ni content were prepared; these were abbreviated as Ni@MCM-x, where 'x' represents the Ni content.

A 'blank' MCM-41 sample was prepared in the same way as reported above, with the exception of no Ni(acac)₂ addition. For comparison, Ni/MCM-41 with 3.0 wt.% Ni content was prepared by a wetness impregnation method with an aqueous solution of Ni(NO₃)₂. Similarly, a

sample of Pt/MCM-41 with 0.3 wt.% Pt content was prepared by impregnation with H₂PtCl₆ solution.

Characterization of catalysts

The Ni content of catalysts was determined by inductively coupled plasma atomic emission spectroscopy (ICP-AES) on an Agilent 710-ES. X-ray diffraction (XRD) data were recorded using Rigaku SmartLab equipment, with Cu K α radiation. N₂ adsorption-desorption isotherms were determined with Belsorp-Max equipment at 77 K. All samples were pretreated at 150 °C in N₂ for 10 h. The surface area and pore volume were calculated using the BET equation. Pore diameter distribution were determined by means of the nonlocal density functional theory (NLDFT) method; the parameters were set as PSD fitting: no assumption, surface element: oxygen, and pore type: cylinder. Average pore size were calculated by BJH. Transmission electron microscopy (TEM) and energy dispersive spectroscopy (EDS) measurements were carried out on a JEOL JEM-2800. UV-vis spectra was recorded with a Nicolet iS-50 spectrometer (Thermo Scientific, Waltham, MA, USA). X-ray photoelectron spectroscopy (XPS) analysis was carried out with an Axis Ultra DLD spectrometer (Kratos Analytical Ltd., UK) equipped with an Al K α X-ray source (250 W). Tests were carried out with an analyzer pass energy of 188 eV for survey scans and 30 eV for detailed elemental scans. The temperature programmed reduction of H₂ (H₂-TPR) and CO pulse chemisorption were determined with a Micromeritics Chemisorb 2750 gas adsorption instrument. For the analysis of H₂-TPR, the NiO@MCM-x sample was pretreated in N₂ at 200 °C for 2 h. In the test process, the samples were heated to 800 °C at a rate of 10 °C min⁻¹, in 10% H₂/Ar. For the measurement of CO pulse chemisorption, the sample was first pretreated in 10% H₂/Ar at 600 °C for 2 h. After the sample had cooled to room temperature, pulses of 10% CO/He in a He carrier (25 mL min⁻¹) were periodically injected at 30 °C, through a loop tube, until the adsorption of the catalyst reached saturation. Dispersion was calculated from CO chemisorption assuming crystallites were hemispherical, a 1:1 stoichiometry (i.e., 1 molecule of CO interacts with one exposed atom of Ni) and the crystallites were reduced.

Determination of Catalytic performance

The HDA activities of Ni@MCM-3 and Ni@MCM-1.5 were determined by hydrogenating naphthalene in a continuous-flow fixed-bed microreactor. For comparison, Ni/MCM-41 (3 wt.% Ni) and Pt/MCM-41 (0.3 wt.% Pt) were also evaluated under with the same conditions. Prior to the reaction, the catalyst was pelleted, crushed, and sieved to 20–40 mesh. It was then loaded into a fixed-bed microreactor and reduced in situ with H₂ flow at 600 °C for 3 h. The reaction material was 5% naphthalene in cyclohexane. Test conditions were the following: pressure 3 MPa, liquid hourly space velocity (LHSV) 1 h⁻¹, and V(H₂)/V(oil) = 600. Liquid products were collected and analyzed with a GC-MS instrument (7890A/5975C; Agilent) equipped with an HP-5 column. The apparent activation energy (*E*_a) was calculated when the naphthalene conversion was < 20% (LHSV 3 h⁻¹), using the Arrhenius empirical equation [equation 1]:

$$\ln \gamma = -\frac{E_a}{RT} + \ln A \quad (1)$$

where γ (mol s⁻¹ g⁻¹) is the reaction rate, R is the universal gas constant, T is the temperature (in Kelvin) and A is the pre-exponential factor. The turnover frequency (TOF) was calculated at 120 °C for LHSV 3 h⁻¹, using the following equation [equation 2]:

$$TOF = \frac{F_{AO}}{W} \frac{X_A}{CO_{uptake}} \quad (2)$$

where *F*_{AO} is the rate of reactant fed into the reactor (μmol h⁻¹), *X*_A is the reactant conversion (%), *W* is the catalyst weight (g), and *CO*_{uptake} is the uptake of chemisorbed CO (μmol g⁻¹).

FULL PAPER

Acknowledgements

This work was financially supported by the NSFC (21878162, 21603107, U1403293), MOE (IRT-13R30 and 113016A), NSFT (16YFZCGX00020), the Research Fund for 111 Project (B12015).

Keywords: decalin • hydrogenation • MCM-41 • nickel • naphthalene

- [1] K. X. Yao, X. Liu, Z. Li, C. C. Li, H. C. Zeng, Y. Han, *ChemCatChem* **2012**, *4*, 1938-1942.
- [2] a) H. Chen, Y. He, L. D. Pfefferle, W. Pu, Y. Wu, S. Qi, *ChemCatChem* **2018**, *10*, 2558-2570; b) W. Alsalahi, W. Tylus, A. M. Trzeciak, *ChemCatChem* **2018**, *10*, 2051-2058; c) X. Shi, X. Wang, X. Shang, X. Zou, W. Ding, X. Lu, *ChemCatChem* **2017**, *9*, 3743-3751.
- [3] S. Naskar, A. Freytag, J. Deutsch, N. Wendt, P. Behrens, A. Köckritz, N. C. Bigall, *Chem. Mater.* **2017**, *29*, 9208-9217.
- [4] E. Kordouli, B. Pawelec, C. Kordulis, A. Lycourghiotis, J. L. G. Fierro, *Appl. Catal. B: Environ.* **2018**, *238*, 147-160.
- [5] a) X. Chen, Y. Ma, L. Wang, Z. Yang, S. Jin, L. Zhang, C. Liang, *ChemCatChem* **2015**, *7*, 978-983; b) Y. Li, Y. Zhao, B. Chen, W. Wang, *ChemCatChem* **2018**, *10*, 2612-2619.
- [6] a) S. Li, A. Tuel, D. Laprun, F. Meunier, D. Farrusseng, *Chem. Mater.* **2015**, *27*, 276-282; b) C. Yu, J. Fu, M. Muzzio, T. Shen, D. Su, J. Zhu, S. Sun, *Chem. Mater.* **2017**, *29*, 1413-1418; c) Q. Fan, X. Li, Z. Yang, J. Han, S. Xu, F. Zhang, *Chem. Mater.* **2016**, *28*, 6296-6304.
- [7] a) L. S. Ribeiro, J. J. Delgado, J. J. M. Órfão, M. F. R. Pereira, *Appl. Catal. B: Environ.* **2017**, *217*, 265-274; b) S. Song, S. Yao, J. Cao, L. Di, G. Wu, N. Guan, L. Li, *Appl. Catal. B: Environ.* **2017**, *217*, 115-124.
- [8] A. Li, T. Wang, X. Chang, W. Cai, P. Zhang, J. Zhang, J. Gong, *Chem. Sci.* **2016**, *7*, 890-895.
- [9] a) X. Song, Q. Guan, Z. Cheng, W. Li, *Appl. Catal. B: Environ.* **2018**, *227*, 13-23; b) C. Y. Ma, B. J. Dou, J. J. Li, J. Cheng, Q. Hu, Z. P. Hao, S. Z. Qiao, *Appl. Catal. B: Environ.* **2009**, *92*, 202-208; c) X. Song, S. Zheng, J. Zhang, W. Li, Q. Chen, B. Cao, *Mater. Res. Bull.* **2012**, *47*, 4305-4310; d) X. Song, Q. Chen, W. Li, J. Zhang, S. Zheng, *Asian. J. Chem.* **2013**, *25*, 2729-2732.
- [10] X. Yang, J.-K. Sun, M. Kitta, H. Pang, Q. Xu, *Nat. Catal.* **2018**, *1*, 214-220.
- [11] J. Zhang, L. Wang, Y. Shao, Y. Wang, B. C. Gates, F. S. Xiao, *Angew. Chem. Int. Ed.* **2017**, *56*, 9747-9751.
- [12] M. Chatterjee, T. Ishizaka, T. Suzuki, A. Suzuki, H. Kawanami, *Green Chem.* **2012**, *14*, 3415-3422.
- [13] X. J. Lin, A. Z. Zhong, Y. B. Sun, X. Zhang, W. G. Song, R. W. Lu, A. M. Cao, L. J. Wan, *Chem. Comm.* **2015**, *51*, 7482-7485.
- [14] A. Mastalir, B. Rác, Z. Király, A. Molnár, *J. Mol. Catal. A: Chem.* **2007**, *264*, 170-178.
- [15] A. K. Medina-Mendoza, M. A. Cortés-Jácome, J. A. Toledo-Antonio, C. Angeles-Chávez, E. López-Salinas, I. Cuauhtémoc-López, M. C. Barrera, J. Escobar, J. Navarrete, I. Hernández, *Appl. Catal. B: Environ.* **2011**, *106*, 14-25.
- [16] V. Danghyan, S. Calderon Novoa, A. Mukasyan, E. E. Wolf, *Appl. Catal. B: Environ.* **2018**, *234*, 178-186.
- [17] C. Wang, Z. Liu, L. Wang, X. Dong, J. Zhang, G. Wang, S. Han, X. Meng, A. Zheng, F.-S. Xiao, *ACS Catalysis* **2017**, *8*, 474-481.
- [18] J. Qin, B. Li, W. Zhang, W. Lv, C. Han, J. Liu, *Micro. Mesop. Mater.* **2015**, *208*, 181-187.
- [19] X. Yang, D. Chen, S. Liao, H. Song, Y. Li, Z. Fu, Y. Su, *J. Catal.* **2012**, *291*, 36-43.
- [20] A. Wong, Liu, Q., Griffin, S., Nicholls, A., Regalbuto, J. R., *sci.* **2017**, *358*, 1427-1430.
- [21] Y. Wang, J. Song, N. C. Baxter, G.-T. Kuo, S. Wang, *J. Catal.* **2017**, *349*, 53-65.
- [22] R. A. Ortega-Domínguez, H. Vargas-Villagrán, C. Peñaloza-Orta, K. Saavedra-Rubio, X. Bokhimi, T. E. Klimova, *Fuel.* **2017**, *198*, 110-122.
- [23] a) M. Luo, Q. Wang, G. Li, X. Zhang, L. Wang, T. Jiang, *Catal. Sci. Technol.* **2014**, *4*, 2081-2090; b) H. Yang, H. Chen, J. Chen, O. Omotoso, Z. Ring, *J. Catal.* **2006**, *243*, 36-42.

FULL PAPER

Entry for the Table of Contents

FULL PAPER

Encapsulation of ultra small Ni particles in the channels of MCM-41. In catalysis hydrogenation of naphthalene, this catalyst shows a high low-temperature activity and excellent selectivity for decalin isomer.



X. Song, Q. Guan,* Y. Shu, X. Zhang, W. Li*

Page No. – Page No.

Facial in situ encapsulation of highly dispersed Ni@MCM-41 for the trans-decalin production from hydrogenation of naphthalene at low temperature